Journal of Quantitative Spectroscopy & Radiative Transfer 147 (2014) 79–85

Contents lists available at ScienceDirect

Journal of Quantitative Spectroscopy & Radiative Transfer

journal homepage: www.elsevier.com/locate/jqsrt

Extending 3D near-cloud corrections from shorter to longer wavelengths

Alexander Marshak [a,*], K. Frank Evans [b], Tamás Várnai [c], Guoyong Wen [d]

[a] NASA Goddard Space Flight Center, Code 613, Greenbelt, MD 20771, USA
[b] Department of Atmospheric and Oceanic Sciences, University of Colorado, 311 UCB, Boulder, CO 80309, USA
[c] JCET/University of Maryland Baltimore County, Baltimore, MD 21228, USA
[d] GESTAR/Morgan State University, Greenbelt, MD 20771, USA

ARTICLE INFO

Article history:
Received 13 February 2014
Received in revised form
21 April 2014
Accepted 7 May 2014
Available online 27 May 2014

Keywords:
Aerosol optical thickness
3D spectral correction for longer wavelengths
Large-Eddy Simulations

ABSTRACT

Satellite observations have shown a positive correlation between cloud amount and aerosol optical thickness (AOT) that can be explained by the humidification of aerosols near clouds, and/or by cloud contamination by sub-pixel size clouds and the cloud adjacency effect. The last effect may substantially increase reflected radiation in cloud-free columns, leading to overestimates in the retrieved AOT. For clear-sky areas near boundary layer clouds the main contribution to the enhancement of clear sky reflectance at shorter wavelengths comes from the radiation scattered into clear areas by clouds and then scattered to the sensor by air molecules. Because of the wavelength dependence of air molecule scattering, this process leads to a larger reflectance increase at shorter wavelengths, and can be corrected using a simple two-layer model [18]. However, correcting *only* for molecular scattering skews spectral properties of the retrieved AOT. Kassianov and Ovtchinnikov [9] proposed a technique that uses spectral reflectance ratios to retrieve AOT in the vicinity of clouds; they assumed that the cloud adjacency effect influences the spectral ratio between reflectances at two wavelengths less than it influences the reflectances themselves. This paper combines the two approaches: It assumes that the 3D correction for the shortest wavelength is known with some uncertainties, and then it estimates the 3D correction for longer wavelengths using a modified ratio method. The new approach is tested with 3D radiances simulated for 26 cumulus fields from Large-Eddy Simulations, supplemented with 40 aerosol profiles. The results showed that (i) for a variety of cumulus cloud scenes and aerosol profiles over ocean the 3D correction due to cloud adjacency effect can be extended from shorter to longer wavelengths and (ii) the 3D corrections for longer wavelengths are not very sensitive to unbiased random uncertainties in the 3D corrections at shorter wavelengths.

Published by Elsevier Ltd.

1. Introduction

There is a positive correlation between cloud amount and aerosol optical thickness (AOT) (e.g., [16,8,31,19]). This correlation can be explained by the humidification of aerosols in the moist cloud environment [23,1] and/or by a transition between aerosol and clouds where the distinction between cloudy and cloud-free air becomes problematic [13]. The correlation is also partly due to remote sensing artifacts such as cloud contamination (e.g., [31,14,27]).

For low clouds, both sub-pixel cloud contamination (e.g., [24,31]) and the cloud adjacency effect (e.g., [12,28,26]) substantially increase reflected radiation, thus leading to

* Corresponding author. Tel.: +1 301 614 6122; fax: +1 301 614 6307.
E-mail address: alexander.marshak@nasa.gov (A. Marshak).

http://dx.doi.org/10.1016/j.jqsrt.2014.05.022
0022-4073/Published by Elsevier Ltd.

significant overestimates of the retrieved AOT. In this paper we focus on the cloud adjacency effect assuming cloud-free columns.

In the vicinity of boundary layer clouds over ocean, the main contribution to the enhancement of clear sky reflectances at shorter wavelengths comes from the radiation scattered into clear areas by clouds and then scattered to the sensor by air molecules [29]. This leads to a larger reflectance increase for shorter wavelengths, or to a "bluing" of aerosols near clouds. Marshak et al. [18] proposed a simple two-layer model to correct for the contribution from enhanced molecular scattering that results from the presence of nearby clouds. This model was recently applied to a full Moderate Resolution Imaging Spectroradiometer (MODIS) granule [30]. However, correcting *only* for molecular scattering skews spectral properties of the retrieved AOT and overcorrects the Ångstrom exponent.

Following a different approach, [9] proposed and further developed [10,11] a technique that uses spectral reflectance ratios to retrieve AOT in the vicinity of clouds. Their main assumption is that the cloud adjacency effect impacts the spectral ratio between reflectances at two wavelengths less than it impacts the reflectances themselves. Thus, the ratio of 3D radiances at two wavelengths λ_1 and λ_2 is approximately equal to the ratio of their 1D counterparts, i.e.

$$R_{3D}(\lambda_1)/R_{3D}(\lambda_2) \approx R_{1D}(\lambda_1)/R_{1D}(\lambda_2) = \rho(\lambda_1, \lambda_2) \tag{1}$$

where $R_{3D}(\lambda)$ and $R_{1D}(\lambda)$ are respectively 3D and 1D radiances at wavelength λ. With three wavelengths (470, 660 and 870 nm), the ratio method uses two independent ratios from which the two parameters of the AOT spectral dependence described by a power-law are retrieved.

Here we combine the two approaches. We assume that the 3D correction for the shortest wavelength (466 nm in this study) is known (with some level of uncertainty). Based on it, we estimate the 3D correction for longer wavelengths (855 nm in this study) using a modified ratio method. We test our new approach of extending the correction from shorter to longer wavelengths with 3D (and 1D) radiances calculated by the Spherical Harmonic Discrete Ordinate Method (SHDOM) for atmospheric radiative transfer [7] for 26 cumulus fields from the UCLA Large-Eddy Simulations (LES) model [22], supplemented with 40 aerosol profiles based on GEOS-5 [21] global reanalysis. Sections 2 and 3 describe our approach and dataset, respectively, Section 4 presents the results, and Section 5 offers a summary and discussion.

2. Approach

Let the observed (normalized) radiance $R_{3D}(\lambda)$ at wavelength λ be represented as a sum of two components: $R_{1D}(\lambda)$ and $\Delta(\lambda)$, i.e.

$$R_{3D}(\lambda) = R_{1D}(\lambda) + \Delta(\lambda). \tag{2a}$$

here $R_{1D}(\lambda)$ is a 1D counterpart of $R_{3D}(\lambda)$ that accounts only for a clear-sky column and ignores any cloud-related adjacency effects. The difference between $R_{3D}(\lambda)$ and $R_{1D}(\lambda)$ is $\Delta(\lambda)$ and will be called a spectral 3D correction. The question we address here is how the 3D correction for longer wavelengths can be estimated from the shorter wavelength correction. For example, if $\Delta(\lambda_1 = 466\text{ nm})$ is known, how $\Delta(\lambda_2 = 855\text{ nm})$ can be assessed. The importance of using shorter wavelength correction for estimating its longer wavelength counterparts follows from our ability to account for the cloud-Rayleigh radiation interaction [18] that dominates for shorter wavelengths over dark surfaces with an aerosol layer predominantly below the cloud tops [29]. Because aerosol properties are unknown, it would be hard to accurately estimate the contribution to the adjacency effect caused by cloud-to-aerosol scattering, which can dominate at longer wavelengths. Thus extending the shorter wavelengths correction into longer wavelengths will improve estimates of the spectral signature of 3D cloud enhancement.

Next we revisit some features of the MODIS aerosol (MOD04) retrieval algorithm [20] that are relevant to this study. First, a cloud masking algorithm removes cloudy pixels within 20 pixel by 20 pixel boxes (with pixel size of 500 m by 500 m each box is 10 km by 10 km). In addition to cloudy pixels, the darkest and brightest 25% are also discarded as likely affected by clouds [15]. The radiances of the remaining 500 m pixels are averaged and the average values are used later for multi-spectral aerosol retrievals. As a result, Eq. (2a) can be modified as

$$R^i{}_{3D}(\lambda) = R_{1D}(\lambda) + \Delta^i(\lambda), \quad i = 1, 2, \ldots, N, \tag{2b}$$

where N is the number of remaining pixels in a 10 km by 10 km box. Note that in order to be used for aerosol retrievals, a 20 by 20 pixel box must have at least 10 (out of 400) remaining pixels, i.e. $N \geq 10$. Here we assumed that R_{1D} does not vary for the selected N pixels.

Let a and b be linear regression coefficients between R^i_{3D} values for two wavelengths in a single 10 km by 10 km box, i.e.

$$R^i{}_{3D}(\lambda_2) \approx aR^i{}_{3D}(\lambda_1) + b, \quad i = 1, 2, \ldots, N. \tag{3a}$$

We assume that $\lambda_1 < \lambda_2$ (e.g., $\lambda_1 = 466$ nm and $\lambda_2 = 855$ nm). For the same two wavelengths, the linear regression for Δ^is can be wr^{i}tten as

$$\Delta^i(\lambda_2) \approx a_\Delta \Delta^i(\lambda_1) + b_\Delta, \quad i = 1, 2, \ldots, N \tag{3b}$$

with regression coefficients a_Δ and b_Δ. Since it was assumed that R_{1D} is constant for the whole 10 km by 10 km box, we expect

$$a_\Delta \approx a. \tag{4a}$$

Indeed,

$$\begin{aligned}\Delta^i(\lambda_2) &= R^i{}_{3D}(\lambda_2) - R_{1D}(\lambda_2) \approx aR^i{}_{3D}(\lambda_1) + b - R_{1D}(\lambda_2)\\ &= a[R_{1D}(\lambda_1) + \Delta^i(\lambda_1)] + b - R_{1D}(\lambda_2)\\ &= a\Delta^i(\lambda_1) + aR_{1D}(\lambda_1) - R_{1D}(\lambda_2) + b.\end{aligned}$$

Comparing this with (3b), we see that $a_\Delta \approx a$ and

$$b_\Delta \approx aR_{1D}(\lambda_1) - R_{1D}(\lambda_2) + b. \tag{4b}$$

Our hypothesis here is that

$$b_\Delta \approx 0 \tag{5a}$$

or, as follows from (5a) and (4b),

$$R_{1D}(\lambda_2) \approx aR_{1D}(\lambda_1) + b. \tag{5b}$$

In reality, because of aerosol small-scale spatial variability (including changing of aerosol particles near clouds), aerosol (and surface) properties are not constant; thus R_{1D} varies inside a 10 km by 10 km box. (Note that for a special case of $b=0$, Eqs. (3a) and (5b) are identical to Eq. (1).)

The linear regression coefficients a and b (as well as a_Δ and b_Δ) for given two wavelengths depend on many factors: solar and viewing geometry, aerosol spectral properties, cloud structure and even surface spectral reflectance. In general, $a_\Delta \neq a$ and $b_\Delta \neq 0$. However, they can be equal approximately, and the validity (and accuracy) of approximations (4a) and (5a) can be tested numerically with realistic models of broken cloud fields. Here we will use models of oceanic trade cumulus clouds and radiance enhancements in aerosol columns due to 3D cloud effects calculated with SHDOM [7].

As a result, if approximations (4a) and (5a) are accurate enough, the unknown 3D correction for longer wavelengths can be approximated from the known correction for shorter wavelength as

$$\Delta^{app}(\lambda_2) = a\Delta(\lambda_1), \tag{6a}$$

and $R_{1D}(\lambda_2)$ can be approximated as

$$R^{app}{}_{1D}(\lambda_2) = R_{3D}(\lambda_2) - \Delta^{app}(\lambda_2) = R_{3D}(\lambda_2) - a\Delta(\lambda_1), \tag{6b}$$

where a is determined from (3a).

3. Data

The UCLA LES model [22] was run for 26 simulations of marine boundary layer cumulus in a 20 km by 20 km domain with horizontal grid spacing of 62.5 m. The LES

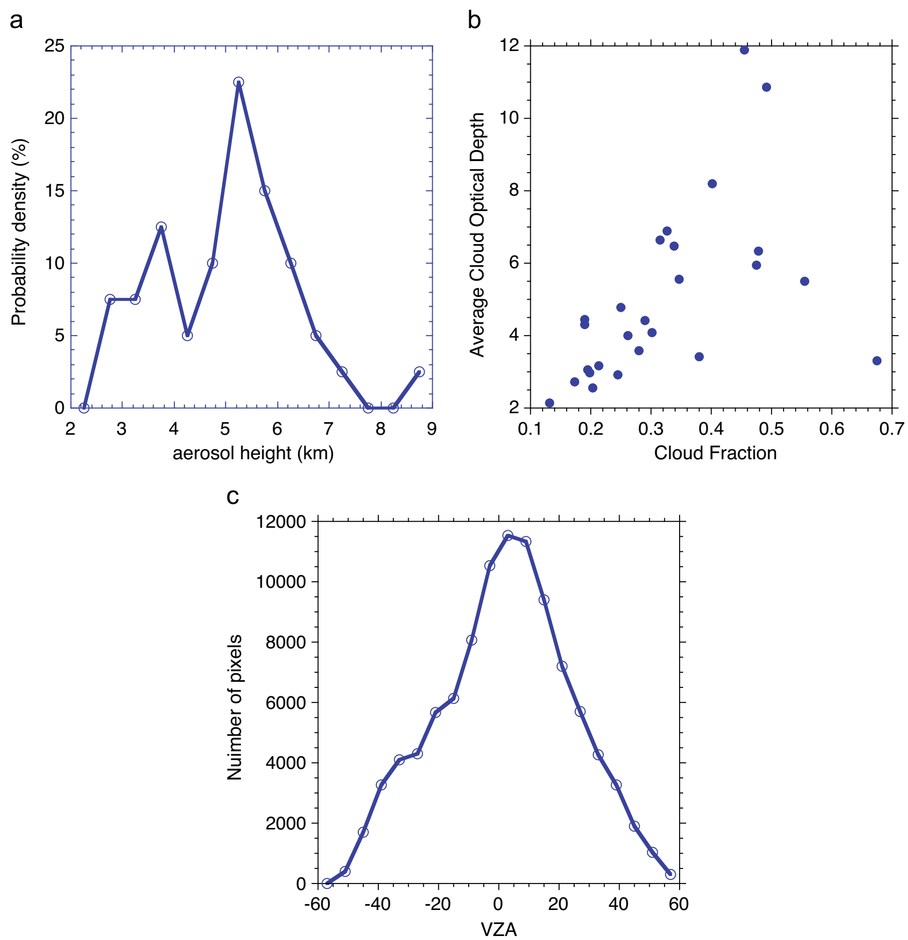

Fig. 1. (a) Distribution of aerosol height weighted with extinction. (b) Average cloud optical depth at 553 nm as a function of cloud fraction (with cloudy 500 m pixels having optical depth4 0.5) for the 26 LES scenes and (c) Number of clear pixels as a function of viewing zenith angles.

cloud microphysics assumes a fixed cloud droplet concentration (chosen randomly from an exponential distribution between 40 and 400 cm^{-3}) and uses a two-moment drizzle/rain bulk microphysics scheme. Each simulation was initialized with a meteorological profile obtained from an ERA-Interim reanalysis [6] column over the northeast Pacific between 2007-05-21 and 2007-09-23. The 3D liquid water content and relative humidity fields at 6 h simulation time were used.

Forty representative aerosol profiles to use with the LES cloud fields were obtained from GEOS-5 [21] global fields over tropical and midlatitude oceans. GEOS-5 has five aerosol types: dust, sea salt, sulfate, black carbon, and organic carbon ([4] and [5]), each with varying number of size bins. The complete aerosol optical properties were calculated from the GEOS-5 optical properties tables as a function of the LES relative humidity. The 40 aerosol profiles were chosen to have a wide range of 550 nm optical depth, single scattering albedo, Angstrom exponent, and extinction weighted mean altitude. The latter is illustrated in Fig. 1a. Each of the 40 aerosol profiles was paired twice with one of the 26 LES cloud scenes to make a total of 80 cloud/aerosol scenes for this study.

Radiances at the LES resolution were calculated with SHDOM [7] for these 80 scenes at the seven MODIS bands used for aerosol remote sensing (wavelengths of 0.466, 0.553, 0.646, 0.855, 1.243, 1.632, and 2.119 um). Rayleigh molecular scattering [2] and molecular absorption from water vapor and ozone were included up to the ~15.6 km domain top. An SHDOM ocean surface reflectance model with the LES surface wind speed was assumed. The solar-viewing geometry was obtained for the LES latitude, date, and the 13:30 local time of the Aqua overpass. SHDOM runs were made for 3D cloud/aerosol fields, 3D hydrated aerosol-only fields, and 1D aerosol-only fields. The radiance differences between these runs show the effects of nearby clouds and variable humidity on the clear pixel aerosol radiances. MODIS 500 m pixels were simulated

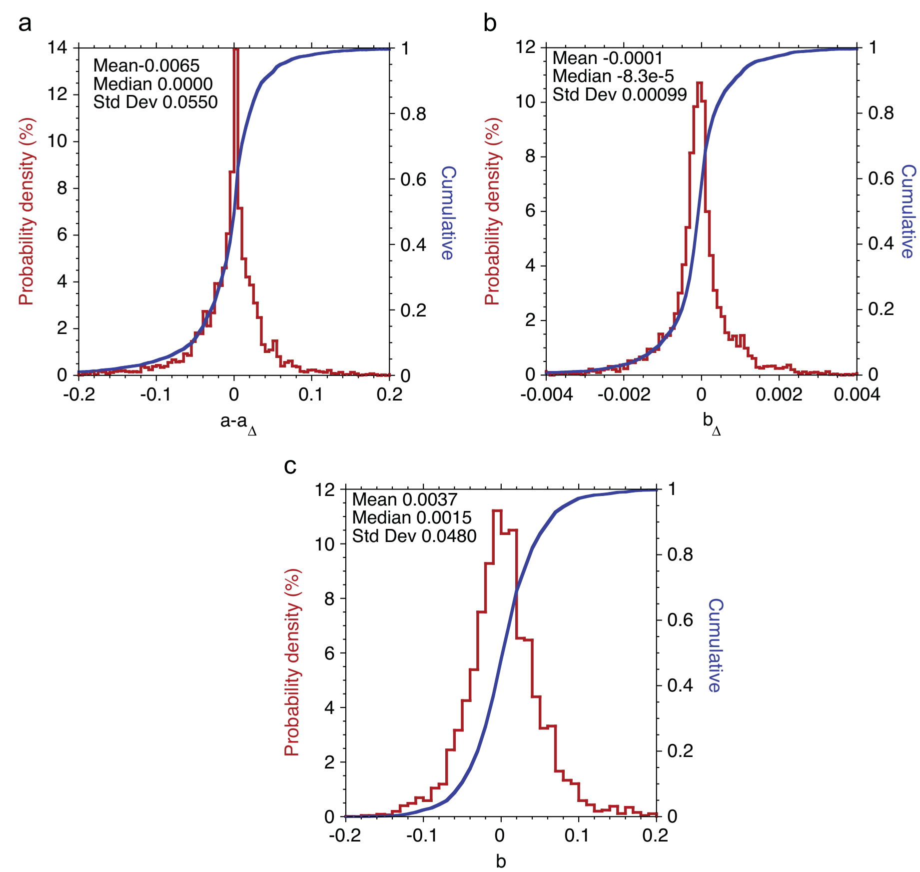

Fig. 2. Probability density and cumulative functions of (a) $a-a_\Delta$, (b) b_Δ and (c) b.

from the SHDOM radiances at 23 viewing directions (at 6° zenith angle spacing) appropriate for MODIS Aqua. Fig. 1b shows the cloud fraction and average cloud optical depth for the 26 LES scenes. Finally, the MODIS Aerosol (MOD04) cloud masking procedure was implemented on the simulated MODIS pixels in 10 km blocks [15].

The total number of 500-m pixels that passed MOD04 cloud masking for all 80 scenes is 100,188, while the total number of 10 km by 10 km boxes is 3154. Note that each scene consists of maximum four 10 km by 10 km boxes, but not all of them have more than ten 500 m by 500 m pixels that passed the cloud masking procedure, especially for high viewing zenith angles (Fig. 1c). Hence the results provided below are slightly biased towards higher sun and lower viewing zenith angles.

4. Results

First we will test numerically the accuracy of the assumptions (4a) and (5a). Fig. 2a shows the probability density function (pdf) and the cumulative function of the differences between a and a_Δ. It confirms that there is no bias (median=0.0) and in 80% of cases $|a-a_\Delta|<0.05$. The average relative difference between a and a_Δ is 2.4%. Fig. 2b illustrates the pdf of b_Δ and its cumulative function. From the cumulative function we can see that in 94% cases $|b_\Delta|<0.002$, in 81% cases $|b_\Delta|<0.001$, and in 64% cases $|b_\Delta|<0.0005$. Finally, Fig. 2c confirms that the b-coefficient from Eq. (3a) is different from 0: in 78% cases $|b|\geq 0.01$, in 24% cases $|b|\geq 0.05$ and in 5% $|b|\geq 0.1$.

Fig. 3a is a scatter plot of $\Delta^{app}(\lambda_2)$ vs. $\Delta(\lambda_2)$ for $\lambda_2=855$ nm. We assume here that the 3D correction for λ_1 is known with some uncertainties. We simulate them by multiplying $\Delta(\lambda_1)$ by $(1+k\xi)$, where k is the maximum uncertainty level and ξ is a uniformly distributed random number between -1 and 1. As follows from Eq. (6a), the multiplicative factor $(1+k\xi)$ applied to $\Delta(\lambda_1)$ can be also interpreted as the one applied to the regression coefficient a. But a is only an approximation to an unknown a_Δ. Based on Fig. 2a, multiplication of a by $(1+k\xi)$ does not bias it, increasing only slightly its standard deviation for $0<k\leq 0.4$. As a result, the unbiased but randomly perturbed $\Delta(\lambda_1)$ does not affect much the accuracy of $\Delta^{app}(\lambda_2)$; Fig. 3a shows almost the same linear fit between $\Delta^{app}(\lambda_2)$ and $\Delta(\lambda_2)$ in all three cases where (i) $\Delta(\lambda_1)$ is known exactly ($k=0$), (ii) $k=0.2$, and (iii) $k=0.4$.

In addition to scatter plot, the pdfs of $\Delta(\lambda_2)-\Delta^{app}(\lambda_2)(1+k\xi)$ and their cumulative counterparts are plotted in Fig. 3b. The cumulative functions for $k=0$ or $k=0.2$ are very similar: quantitatively in these two cases 83% of all pixels have $|\Delta^{app}(\lambda_2)-\Delta(\lambda_2)(1+k\xi)|<0.001$ and 63% pixels have $|\Delta^{app}(\lambda_2)-\Delta(\lambda_2)(1+k\xi)|<0.0005$ (for $k=0.4$ these numbers are slightly lower: 81% and 59%, respectively.)

The difference between $R_{3D}(\lambda_2)$ and its approximations (the corrected 3D and the 1D ones) are plotted vs. $R_{3D}(\lambda_2)$ in Fig. 4a. While the 1D approximation is biased low, the 3D correction is uniformly distributed around the true values of $R_{3D}(\lambda_2)$. This is confirmed with their pdfs plotted in Fig. 4b. Note that the pdfs of $R_{3D}(\lambda_2)-R^{app}_{3D}(\lambda_2)$ plotted in Fig. 4b are identical to pdfs of $\Delta(\lambda_2)-\Delta^{app}(\lambda_2)$ plotted in Fig. 3b since,

$$R_{3D}(\lambda_2)-R^{app}{}_{3D}(\lambda_2)=[R_{1D}(\lambda_2)+\Delta(\lambda_2)]-[R_{1D}(\lambda_2)+\Delta^{app}(\lambda_2)]$$
$$=\Delta(\lambda_2)-\Delta^{app}(\lambda_2).$$

In addition to $k=0$, 0.2 and 0.4, Fig. 4b also shows the case with $k=0.8$. As we see, the uncertainties in $\Delta(\lambda_1)$ bias $R^{app}_{3D}(\lambda_2)$ (or $\Delta^{app}(\lambda_2)$) only slightly. Quantitatively, means (and standard deviations) of the differences are 6.4×10^{-5} (0.0010), 6.4×10^{-5} (0.0011), 6.5×10^{-5} (0.0012), 6.3×10^{-5} (0.0015) for $k=0.0$, 0.2, 0.4 and 0.8, respectively, while for the difference with 1D approximation the mean is 0.0016 and the standard deviation is 0.0014.

Finally, we note that as follows from Eq. (6b), our goal is to estimate the unknown $R_{1D}(\lambda_2)$ (or $\Delta^{app}(\lambda_2)$) rather than $R_{3D}(\lambda_2)$, which is measured and does not need to be approximated. However, here the accuracy of $R^{app}_{1D}(\lambda_2)$ approximation was illustrated using the comparison

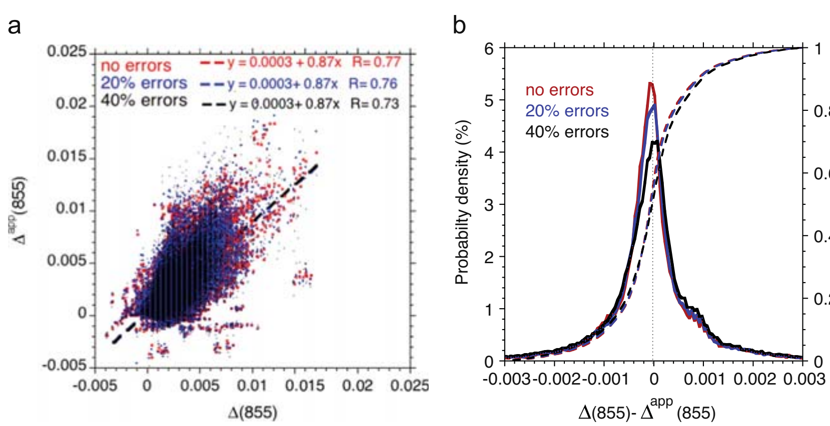

Fig. 3. (a) Scatter plot of $\Delta^{app}(\lambda_2)$ determined from $\Delta(\lambda_1)$ using Eq. (6a) vs. the "true" $\Delta(\lambda_2)$ where $\lambda_1=466$ nm and $\lambda_2=855$ nm. The unbiased uniformly distributed random uncertainties with maximum of 20% (blue) and 40% (black) have been added to $\Delta(\lambda_1)$, and (b) Probability density and cumulative functions of $\Delta(\lambda_2)-\Delta^{app}(\lambda_2)$.

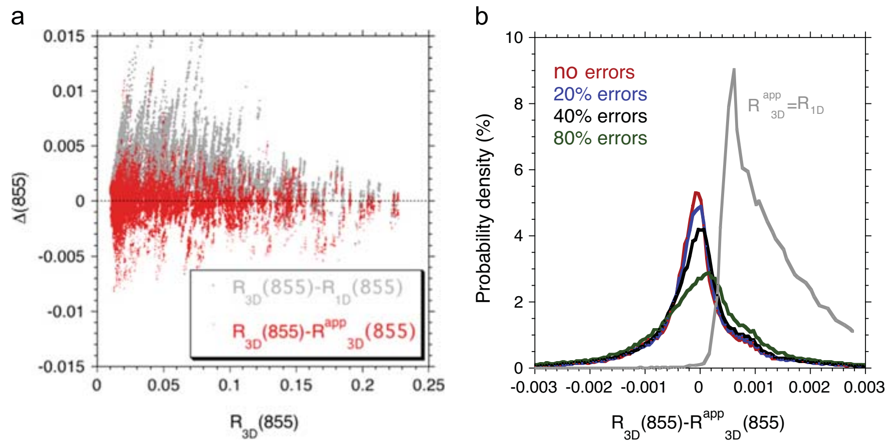

Fig. 4. (a) The difference between $R_{3D}(\lambda_2)$ and its two approximations: $R_{3D}^{app}(\lambda_2)=R_{1D}(\lambda_2)+a\Delta(\lambda_1)$ (red) and $R_{1D}(\lambda_2)$ (gray) vs. $R_{3D}(\lambda_2)$. (b) Probability density functions of $R_{3D}(\lambda_2)-R_{3D}^{app}(\lambda_2)$ for 5 cases: $\Delta(\lambda_1)$ known exactly; with maximum of 20%, 40%, 80% random unbiased uncertainties, and the case of $R_{3D}^{app}(\lambda_2)=R_{1D}(\lambda_2)$. As in the other figures, $\lambda_1=466$ nm and $\lambda_2=855$ nm.

between $R_{3D}^{app}(\lambda_2)$ and $R_{3D}(\lambda_2)$ which is the same as the difference between $R_{1D}^{app}(\lambda_2)$ and $R_{1D}(\lambda_2)$.

5. Summary and discussion

Ignoring 3D radiative cloud adjacency effects is one of the main sources of errors in remote sensing retrievals of aerosol properties in cloud-free columns [13,14,26]. Preventing these errors by excluding the retrieved aerosols near clouds will dramatically reduce the database and underestimate the aerosol radiative forcing, while including these areas may overestimate the forcing because of unaccounted cloud contamination. Many studies discussed this problem (e.g., [3,17,25]) but only few proposed ways to account for the effect [18,29,30,9–11]. So far none of them has reached a level of maturity for operational use.

This paper combines the earlier approaches proposed in Marshak et al. [18] and Kassianov and Ovchinnikov [9]. First, based on Marshak et al.'s paper, it is assumed here that we can successfully correct for 3D radiative effects at shorter wavelengths, where cloud–Rayleigh interactions dominate the radiation enhancement in cloud-free columns. Second, we use the Kassianov and Ovchinnikov approach, but instead of Eq. (1), we assume Eqs. (3a) and (5b). The early and new assumptions would be similar if $b=0$, but it is not (see Fig. 2c). Third, in contrast to Kassianov and Ovchinnikov's approach, we do not retrieve AOT but only correct reflectances for the cloud adjacency effect. Thus we do not use the assumption of a power-law spectral representation of AOT that may be too restrictive.

The proposed correction algorithm for a 10 km × 10 km box is the following:

(i) At the shortest available wavelength λ_1, get the correction □(λ_1) for cloud-Rayleigh interaction using the “two-layer” model of Marshak et al. [18].

(ii) For a longer wavelength λ_2, get a linear regression coefficient a relating $R_{3D}^{i}(\lambda_2)$ to $R_{3D}^{i}(\lambda_1)$ as in Eq. (3a) for all 500 m pixels kept by the MODIS operational cloud masking algorithm.

(iii) Estimate $\Delta(\lambda_2)$ as a product of a and $\Delta(\lambda_1)$ and subtract it from measured $R_{3D}(\lambda_2)$ as in Eq. (6b).

(iv) Repeat the above correction for all other wavelengths $\lambda 4\ \lambda_1$ used in the MODIS spectral AOT retrieval algorithm.

(v) Finally, apply the MODIS AOT retrieval algorithm to the estimated 1D reflectances—that is, to the differences between $R_{3D}(\lambda)$ and $\Delta(\lambda)$ for all bands.

Note that the assumptions of dark surface and the aerosol layers below cloud top are applied only to our simple two-layer model (step (i)) and are not used with other steps of the algorithm proposed in this paper. The two-layer model has not been yet thoroughly validated. The results of validation will be reported elsewhere.

To test our approach, we used 26 cumulus cloud fields (20 km by 20 km each) generated with the UCLA LES model, and combined them with 40 aerosol profiles based on GEOS-5 [21] global reanalysis. Radiances for 80 scenes were calculated using SHDOM [7] for two MODIS bands ($\lambda_1=0.466$ □m and $\lambda_2=0.855$ □m) and 23 viewing directions. Radiances were averaged to 500 m resolution, and the MODIS aerosol cloud masking procedure was implemented on 10 km boxes [15]. The total number of 10 km by 10 km boxes was 3154 and the total number of 500 m by 500 m pixels that passed MOD04 cloud masking in all 80 scenes and for 23 view directions was 100,188.

The results showed that (i) for a variety of cumulus cloud scenes and aerosol profiles over dark ocean surfaces, the 3D correction due to cloud adjacency effect can be successfully extended from shorter to longer wavelengths and (ii) the 3D corrections at longer wavelengths are not

very sensitive to random unbiased uncertainties in the 3D corrections at shorter wavelengths.

Acknowledgments

This research was supported by the Office of Science (Biological and Environmental Research, US Department of Energy, Interagency Agreement no. DE-AI02-08ER64562) as part of the ASR program and by the NASA Radiation Sciences Program managed by Hal Maring. We also thank Drs. Robert Levy and Alexei Lyapustin for fruitful discussions, valuable comments, and suggestions.

References

[1] Bar-Or RZ, Koren I, Altaratz O, Fredj E. Radiative properties of humidified aerosols in cloudy environment. Atmos Res 2012;118:280–94.
[2] Bodhaine BA, Wood NB, Dutton EG, Slusser JR. On Rayleigh optical depth calculations. J Atmos Oceanic Technol 1999;16:1854–61.
[3] Charlson R, Ackerman A, Bender F, Anderson T, Liu Z. On the climate forcing consequences of the albedo continuum between cloudy and clear air. Tellus 2007;59:715–27.
[4] Chin M, Ginoux P, Kinne S, Torres O, Holben BN, Duncan BN, et al. Tropospheric aerosol optical thickness from the GOCART model and comparisons with satellite and sun photometer measurements. J Atmos Sci 2002;59:461–83.
[5] Colarco P, da Silva A, Chin M, Diehl T. Online simulations of global aerosol distributions in the NASA GEOS4 model and comparisons to satellite and ground-based aerosol optical depth. J Geophys Res 2010;115:D14207. http://dx.doi.org/10.1029/2009JD012820.
[6] Dee DP, Uppala S. Variational bias correction of satellite radiance data in the ERA-Interim reanalysis. Quart J R Meteorol Soc 2009;135:1830–41.
[7] Evans KF. The spherical harmonic discrete ordinate method for three-dimensional atmospheric radiative transfer. J Atmos Sci 1998;55:429–46.
[8] Ignatov A, Minnis P, Loeb N, Wielicki B, Miller W, Sun-Mack S, et al. Two MODIS aerosol products over ocean on the Terra and Aqua CERES SSF. J Atmos Sci 2005;62:1008–31.
[9] Kassianov EI, Ovtchinnikov M. On reflectance ratios and aerosol optical depth retrieval in the presence of cumulus clouds. Geophys Res Lett 2008;35:L06807. http://dx.doi.org/10.1029/2008GL033231.
[10] Kassianov EI, Ovtchinnikov M, Berg LK, McFarlane SA, Flynn CJ. Retrieval of aerosol optical depth in vicinity of broken clouds from reflectance ratios: sensitivity study. J Quant Spectrosc Radiat Transf 2009;110:1677–89.
[11] Kassianov EI, Ovchinnikov M, Berg LK, McFarlane SA, Flynn CJ, Ferrare R, et al. Retrieval of aerosol optical depth in vicinity of broken clouds from reflectance ratios: case study. Atmos Meas Technol 2010;3:1333–49. http://dx.doi.org/10.5194/amt-3-1333-2010.
[12] Kobayashi T, Masuda K, Sasaki M, Mueller J. Monte Carlo simulations of enhanced visible radiance in clear-air satellite fields of view near clouds. J Geophys Res 2000;105:26569–76.
[13] Koren I, Remer LA, Kaufman YJ, Rudich Y, Martins JV. On the twilight zone between clouds and aerosols. Geophys Res Lett 2007;34:L08805. http://dx.doi.org/10.1029/2007GL029253.
[14] Koren I, Feingold G, Jiang H, Altaratz O. Aerosol effects on the inter-cloud region of a small cumulus cloud field. Geophys Res Lett 2009;36:L14805. http://dx.doi.org/10.1029/2009GL037424.
[15] Levy RC, Remer LA, Kleidman RG, Mattoo S, Icholu C, Kahn R, et al. Global evaluation of the Collection 5 MODIS dark-target aerosol products over land. Atmos Chem Phys 2010;10:10399–420.
[16] Loeb NG, Manalo-Smith N. Top-of-atmosphere direct radiative effect of aerosols over global oceans from merged CERES and MODIS observations. J Clim 2005;18:3506–26. http://dx.doi.org/10.1175/JCLI3504.1.
[17] Loeb NG, Schuster GL. An observational study of the relationship between cloud, aerosol and meteorology in broken low-level cloud conditions. J Geophys Res 2008;113:D14214. http://dx.doi.org/10.1029/2007JD009763.
[18] Marshak A, Wen G, Coakley J, Remer L, Loeb NG, Cahalan RF. A simple model for the cloud adjacency effect and the apparent bluing of aerosols near clouds. J Geophys Res 2008;113:D14S17. http://dx.doi.org/10.1029/2007JD009196.
[19] Matheson MA, Coakley Jr. JA, Tahnk WR. Aerosol and cloud property relationships for summertime stratiform clouds in the northeastern Atlantic from AVHRR observations. J Geophys Res 2005;110:D24204. http://dx.doi.org/10.1029/2005JD006165.
[20] Remer LA, Kaufman YJ, Tanre D, Mattoo S, Chu DA, Martins JV, et al. The MODIS aerosol algorithm, products and validation. J Atmos Sci 2005;62:947–73.
[21] Rienecker MM, Suarez MJ, Gelaro R, Todling R, Bacmeister J, Liu E, et al. MERRA: NASAs modern-era retrospective analysis for research and applications. J Clim 2011;24:3624–48.
[22] Stevens B, Moeng C-H, Sullivan PP. Large-Eddy Simulations of radiatively driven convection: sensitivities to the representation of small scales. J Atmos Sci 1999;56:3963–84.
[23] Su W, Schuster GL, Loeb NG, Rogers RR, Ferrare RA, Hostetler CA, et al. Aerosol and cloud interaction observed from high spectral resolution lidar data. J Geophys Res 2008;113:D24202, http://dx.doi.org/10.1029/2008JD010588.
[24] Torres O, Bhartia PK, Herman JR, Syniuk A, Ginoux P, Holben B. A long term record of aerosol optical depth from TOMS observations and comparison to AERONET measurements. J Atmos Sci 2002;59:398–413.
[25] Twohy CH, Coakley Jr. JA, Tahnk WR. Effect of changes in relative humidity on aerosol scattering near clouds. J Geophys Res 2009;114:D05205. http://dx.doi.org/10.1029/2008JD010991.
[26] Varnai T, Marshak A. MODIS observations of enhanced clear sky reflectance near clouds. Geophys Res Lett 2009;36:L06807, http://dx.doi.org/10.1029/2008GL037089.
[27] Varnai T, Marshak A, Yang W. Multi-satellite aerosol observations in the vicinity of clouds. Atmos Chem Phys 2013;13:3899–908. http://dx.doi.org/10.5194/acp-13-3899-2013.
[28] Wen G, Marshak A, Cahalan RF, Remer LA, Kleidman RG. 3-D aerosol-cloud radiative interaction observed in collocated MODIS and ASTER images of cumulus cloud fields. J Geophys Res 2007;112:D13204. http://dx.doi.org/10.1029/2006JD008267.
[29] Wen G, Marshak A, Cahalan RF. Importance of molecular Rayleigh scattering in the enhancement of clear sky radiance in the vicinity of boundary layer cumulus clouds. J Geophys Res 2008;113:D24207. http://dx.doi.org/10.1029/2008JD010592.
[30] Wen G, Marshak A, Levy R, Remer L, Loeb N, Varnai T, et al. Implementation of the correction algorithm of the MODIS aerosol retrievals near clouds. J Geophys Res 2013:118. http://dx.doi.org/10.1002/jgrd.50617.
[31] Zhang J, Reid JS, Holben BN. An analysis of potential cloud artifacts in MODIS over ocean aerosol optical thickness product. Geophys Res Lett 2005;32. http://dx.doi.org/10.1029/2005GL023254.